

Tuning brittleness in multi-component metallic glasses through chemical disorder aging

Kamran Karimi^{1*} and Stefanos Papanikolaou^{1†}

¹ *NOMATEN Centre of Excellence,
National Center for Nuclear Research,
ul. A. Soltana 7, 05-400 Swierk/Otwock, Poland*

Shear localization in slowly-driven bulk metallic glasses (BMGs) is typically accompanied by a sharp drop in the bulk stress response as a signature of the plastic yielding transition. It is also observed that the sharpness of this elastic-plastic dynamical transition depends on the extent of local chemical and microstructural orders, as well as the glass preparation protocol (*ie.* thermal annealing). Here, we investigate sheared multi-element BMGs in molecular dynamics (MD) simulations, and demonstrate that glass aging, implemented through a hybrid Monte-Carlo(MC)-MD process, sharpens the elastic-plastic transition through a distinct crossover, seen in strain patterns that gradually shift from diffuse features in as-quenched samples to localized (yet system-spanning) patterns in well-annealed glasses. This effect of glass aging on the elastic-plastic transition is found to be correlated to the inherent interplay between aging-induced icosahedra ordering and co-operative formation of shear transformation zones. The observed crossover is quantified through a measure of the age-dependent susceptibility to plastic rearrangements, exhibiting strong (anti-)correlations to local ordering features, and the corresponding spatial correlation length grows with the aging timescale.

Plastic yielding in slowly sheared metallic glasses (below the glass transition temperature T_g) typically occurs via localization of intense, irrecoverable deformation, yet without crushing or crumbling within the bulk. Microstructurally, this flow is attributed to emergent shear transformation zones (STZs) [1–4], commonly known as carriers of amorphous plasticity, somewhat analogously to dislocations in crystals. STZs mutually interact, as they are soft mesoscale defects that relax stress locally but can further induce far-field elastic-type triggering elsewhere within the glassy medium. This phenomenon leads to *collective* dynamics upon failure and *universal* features, including scale-free statistics and diverging length, time, and/or energy scales that could be understood within the broad context of far-from-equilibrium critical phenomena [5–8]. Despite the observed universality, the *sharpness* of the elastic-plastic transition (seen for example, as a discontinuous stress drop in displacement-controlled uniaxial loading), may exhibit significant variations across multi-element BMGs owing to modifications in thermal treatments (*i.e.* aging/annealing) and chemical compositions [9–12]. In this paper, we concentrated on the equiatomic CoNiCrFeMn alloy that has been commonly regarded in the literature as a high-entropy “Cantor” alloy [13, 14] but we consider only its mechanical properties in the glassy state achieved by fast cooling [15]. We investigate the inherent correlations between microstructure and shear localization, as the amorphous state is gradually aging.

Amorphous metals have the capability to undergo plastic flow mediated by STZs, contributing significantly to

their ductility [16–19]. However, in certain aged glasses, which do not possess inherent heterogeneities [10, 20, 21], or when the associated length scales do not significantly surpass the average interatomic distance, plastic distortion displays localization within a dominant band and eventually brittle-type fracture. This is akin to the ductile-to-brittle transition present in a broad range of amorphous solids [5]. In addition, aging-mediated, structural relaxation, leads to “annealed” metallic glasses that nucleate certain quasi-ordered phases characterized by short range order (SRO) [22–25], and there exists a strong tendency to tune the extent of shear localization through structural ordering [20, 26, 27]. SROs are commonly identified by the formation of ordered icosahedral clusters, representing the most (energetically) favored atomic arrangement within the chemically diverse, amorphous matrix. Such clusters play a pivotal role in developing a number of glassy properties, such as the dynamic slowing-down in the super-cooled regime [28]. It is worth noting that SROs serve as “infertile” sites for the nucleation of STZs in that the latter are typically loosely-packed, soft, and disordered arrangements that weaken the local strength and, thus, enhance the nucleation probability of shear banding instabilities.

In this paper, we investigate the precise characteristics of the inherent SRO-STZ interplay and relevant atomistic mechanisms that influence the nucleation dynamics of shear bands in concentrated and chemically complex BMGs. Previously [19, 29], in concentrated BMGs, we showed how the elastic-plastic transition sharpness and fine-scale structural ordering features in shear bands might be dependent on the chemical composition. Here, we show how room temperature thermal aging may affect four chemically complex glasses and then, we focus on the structural aspects of the transition in the

* kamran.karimi@ncbj.gov.pl

† stefanos.papanikolaou@ncbj.gov.pl

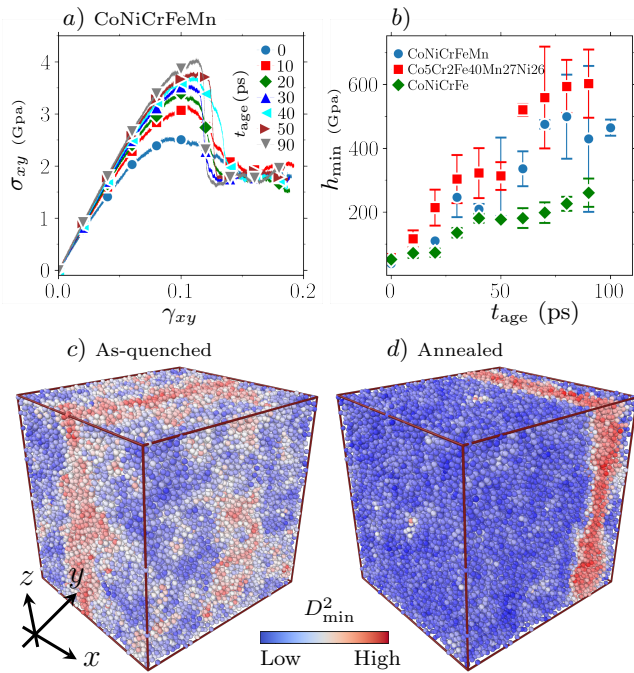


FIG. 1. **a)** Macroscopic stress σ_{xy} plotted against applied (shear) strain γ_{xy} in deforming CoNiCrFeMn annealed at different duration t_{age} **b)** softening modulus h_{min} versus annealing duration t_{age} corresponding to several BMGs. Local mean-squared nonaffine displacements D_{min}^2 associated with **c)** as-quenched ($t_{\text{age}} = 0$) and **d)** annealed ($t_{\text{age}} = 90$ ps) CoNiCrFeMn at $\gamma_{xy} = 0.2$. Here x , y , and z denote flow, gradient, and vorticity directions, respectively. The blue and red colors in **c)** and **d)** indicate low and high D_{min}^2 values, respectively. The size of the cubic box is $L \simeq 80$ Å.

CoNiCrFeMn metallic glass. We center our approach on a classification pertinent to the plastic yielding transition in metallic glasses: *i)* the “good” or annealed glass, forms localized deformation patterns and displays a discontinuous transition in the macroscopic average stress response, *ii)* the “bad” or quenched glass, may delocalize strain and display ductility characteristics. We demonstrate that annealing effectively controls the crossover from bad to good glass by tuning the level of icosahedra-based structural ordering within the glass, thereby influencing its propensity to form shear bands. We perform cluster analysis for a measure that measures non-affine plastic rearrangements, and we show that the cluster correlation length evolves across the yielding transition and exhibits significant variations with sample age.

Simulations & Protocols – The details of the hybrid Monte Carlo (MC) - Molecular Dynamics (MD) simulations, in this work, are given in the Supplementary Material (SM) [30] (see also references [31–35] therein) including the description of relevant units, the preparation protocol, the utilized interatomic potential functions, and also, the deformation parameters of the investigated model metallic glasses [19]. Prior to shearing, the as-quenched samples were subject to MC-MD annealing

up to the aging duration of $t_{\text{age}} = 100$ ps (with standard heuristic assumptions on the MC-related timescale). Simple shear tests were subsequently performed on the aged glasses at a fixed strain rate $\dot{\gamma}_{xy} = 10^{-4}$ ps $^{-1}$ and temperature $T = 300$ K, up to shear strain $\gamma_{xy} = 0.2$. To probe the dynamics of individual atoms, we track the mean squared displacements D_{min}^2 as a measure of atoms’ non-affinity with respect to the imposed shear deformation [2]. We further perform a Voronoi analysis using OVITO [36] to locate atoms displaying icosahedral order, namely polyhedral cells with exactly twelve faces, including regular pentagons. To obtain the associated (number) density, $\rho_{\text{ico}} = 1/V_{\text{ico}}$, we repeat the Voronoi analysis by including *exclusively* atoms with icosahedral symmetries within the periodic box (and excluding other atoms). This gives another set of Voronoi cells with volume V_{ico} . The mean number density of icosahedral clusters is further derived as $\langle \rho_{\text{ico}} \rangle$.

Further, we measure the softening modulus h_{min} , defined as the maximum *rate* of the macroscopic average stress drop at every age t_{age} as in Fig. S3. This stress drop is typically defined as the difference between the overshoot stress and the subsequent flow stress, and is associated with the initiation of a spanning shear band, thus it has been used as an order parameter in model glass studies [5, 37] showing meaningful variations with glass compositions and processing parameters [10]. Nevertheless, in metallic glass simulations and/or experiments, a robust measurement of the macroscopic drop is not always feasible due to the lack of a well-defined steady flow regime beyond the apparent stress overshoot. In a recent work [19], we established h_{min} as a more robust experimentally-relevant indicator of the elastic-plastic transition in BMGs, shear banding and associated structural features.

Results – Figure 1 displays results of the shear tests performed on the aged CoNiCrFeMn glass. The resulting stress-strain curves, σ_{xy} against γ_{xy} in Fig. 1(a), indicate a pronounced stress overshoot, namely a monotonic increase of stress towards a peak value at $\gamma_{\text{max}} \simeq 0.1$, followed by a shear reduction in stress, and prior to a well-defined plastic flow regime, with marked dependence on glass aging. This is quantified in Fig. 1(b) where the rate of stress drop h_{min} tends to grow (and eventually saturate) with increasing t_{age} corresponding to CoNiCrFeMn as well as Co₅Cr₂Fe₄₀Mn₂₇Ni₂₆, CoNiCrFe, and CoNiFe. This feature appears to be quite robust with respect to variations in the chemical composition and/or molar concentrations. The observed enhancement in the sharpness of yielding transition aligns closely with the D_{min}^2 maps as visualized in Fig. 1(b) and (c) corresponding to the as-quenched ($t_{\text{age}} = 0$) and annealed ($t_{\text{age}} = 90$ ps) glasses at $\gamma_{xy} = 0.2$. Notably, the abrupt stress drop in the aged metallic glass is accompanied by localized (and system-spanning) features as illustrated in Fig. 1(d), whereas the as-quenched sample displays scattered deformation patterns across the medium, as in Fig. 1(c).

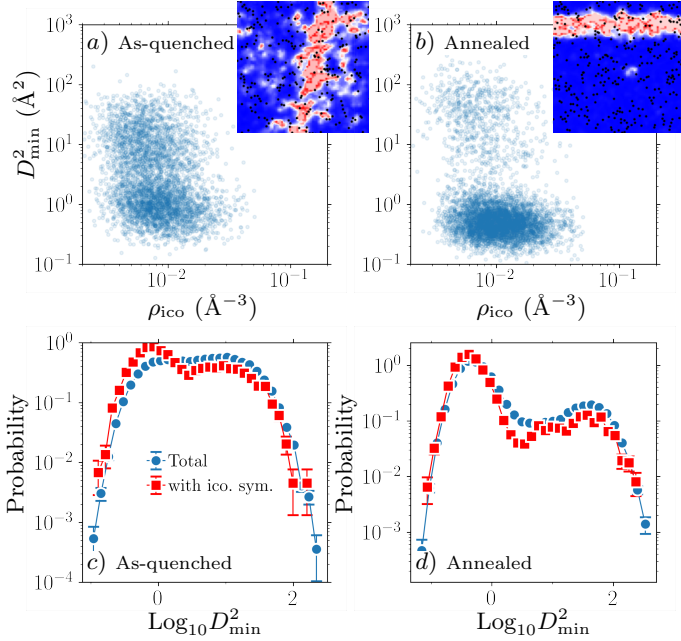


FIG. 2. Scatter plots of D_{\min}^2 and icosahedra density ρ_{ico} in the **a)** as-quenched ($t_{\text{age}} = 0$) and **b)** annealed ($t_{\text{age}} = 90$ ps) CoNiCrFeMn at $\gamma_{xy} = 0.2$. D_{\min}^2 probability distribution function of atoms with the full icosahedral order corresponding to the **c)** as-quenched and **d)** annealed glasses at $\gamma_{xy} = 0.2$. The corresponding D_{\min}^2 spatial maps are shown in the insets with the blue and red colors indicating spatial regions with low and high nonaffine displacements. The (black) dots denote atoms with full icosahedral order. The scale of the color map is $L \simeq 80$ Å.

Here, the blue and red colors in the deformation maps indicate regions with low and high squared nonaffine displacements.

We now turn to the characteristics of microstructural ordering and the interplay with shear bands in the specific, for clarity purposes, deforming metallic glass CoNiCrFeMn. The color maps in the insets of Fig. 2(a) and (b) overlay atoms with the full icosahedral order (black disks) on the two-dimensional (interpolated) D_{\min}^2 field associated with the as-quenched ($t_{\text{age}} = 0$ ps) and annealed ($t_{\text{age}} = 90$ ps) metallic glass at $\gamma_{xy} = 0.2$. It is evident from both maps that (red) rearranging zones notably lack local structural ordering in contrast to the (blue) rigid matrix. This is further illustrated in Fig. 2(c) and (d) displaying D_{\min}^2 probability distribution functions corresponding to atoms with icosahedral symmetry in the as-quenched and annealed sample, respectively. The latter exhibits a clear bimodal behavior in Fig. 2(d) with the first (higher) and second (lower) peaks denoting the population of atoms outside and within shear zones. The conditional distribution (red squares) indicates a relatively higher contribution of the ordered icosahedral phase to the higher peak in very close agreement with the observation of rare ordering occurrences within plastically deforming zones. Such features are also present in Fig. 2(c) corresponding to the as-quenched glass but

with less pronounced bimodality.

Next, we consider the atoms with icosahedral ordering and we carry out a cross correlation analysis between associated squared non-affine displacements and the number density ρ_{ico} . The scatter data of D_{\min}^2 and ρ_{ico} in Fig. 2(a) and (b) indicate significant (anti-)correlations between the two observables $X = \log_{10} D_{\min}^2$ and $Y = \log_{10} \rho_{\text{ico}}$. The (linear) correlation coefficient $c_{XY} = \langle \hat{X}\hat{Y} \rangle$ and its evolution with strain is shown in Fig. 3(a) where $\langle \cdot \rangle_i$ denotes averaging over the atom index i and \hat{X} indicates the deviation from the mean $\langle X \rangle_i$, normalized by the standard deviation associated with each variable. Overall, (anti-)correlation monotonically grows with loading, and it saturates at the onset of the plastic flow regime. The aging process leads to a sharp elastic-plastic transition on approach to failure (see Fig. 1(a) and (b), with a very infrequent occurrence of structural icosahedral ordering within the shear bands (regions with large D_{\min}^2) (cf. Fig. 2(d)).

The aging-induced crossover is also manifested in the evolution of $\langle D_{\min}^2 \rangle$ (averaged over atoms) with t_{age} as in Fig. 3(c). Non-affine displacements are low at small strains but exhibit a clear crossover with increasing age at the onset of yielding ($\gamma_{xy} \simeq 0.1$) above which $\langle D_{\min}^2 \rangle$ grows almost linearly with strain, irrespective of t_{age} . Figure 3(d) displays the scaled standard deviation associated with atoms' D_{\min}^2 as a measure of susceptibility. The overall trend we observe is akin to the behavior illustrated in Fig. 3(c). In this context, fluctuations tend

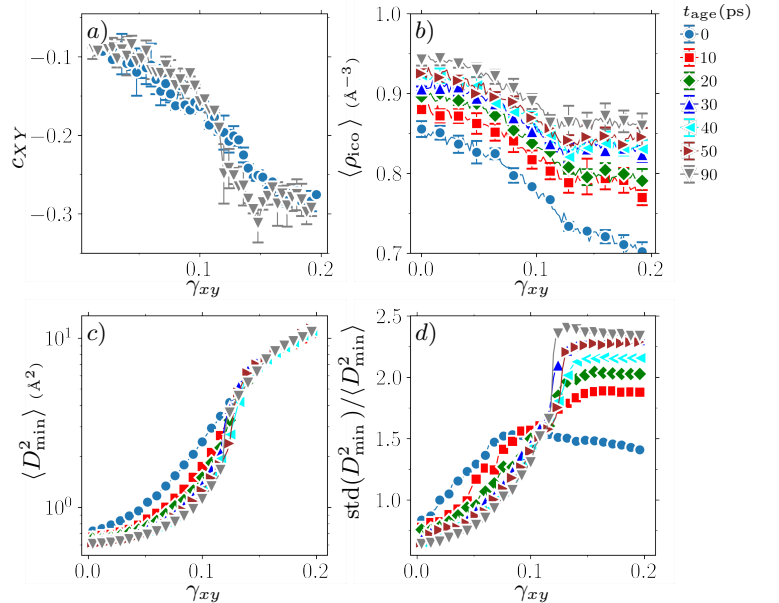


FIG. 3. Evolution of **a)** correlation coefficient c_{XY} **b)** mean number density of atoms with icosahedral symmetries $\langle \rho_{\text{ico}} \rangle$ **c)** mean squared nonaffine displacements $\langle D_{\min}^2 \rangle$ **d)** scaled standard deviation $\text{std}(D_{\min}^2)/\langle D_{\min}^2 \rangle$ associated with atoms' D_{\min}^2 plotted against applied strain γ_{xy} in CoNiCrFeMn corresponding to different aging duration t_{age} . The error bars denote standard errors.

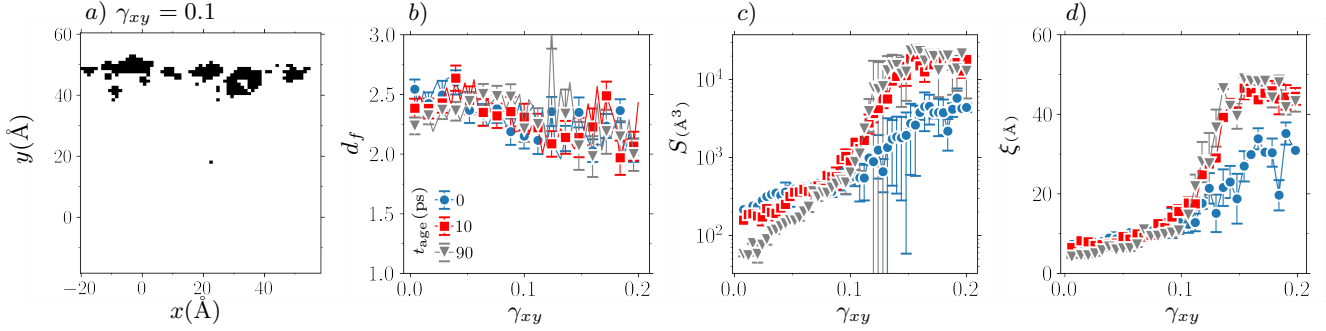


FIG. 4. **a)** Binary D_{\min}^2 map at $\gamma_{xy} = 0.1$ corresponding to the annealed CoNiCrFeMn at $t_{\text{age}} = 90$ ps. **b)** Fractal dimension d_f **c)** Mean cluster size S **d)** Correlation length ξ plotted against strain γ_{xy} at multiple age t_{age} . Here x and y denote flow and gradient directions, respectively. The binary maps show top 5% sites with largest D_{\min}^2 in black.

to reveal an age-dependent shear-induced transition that displays characteristics akin to critical phenomena and a diverging correlation length (*cf.* Fig. 3(d)). The character/order of this shear-induced transition and the exponents associated to this correlation length divergence may be unveiled through finite-size scaling studies in the strong aging regime, a study that goes beyond the purpose of the current work. We also probed variations in the (mean) number density of ordered clusters $\langle \rho_{\text{ico}} \rangle$ with strain as in Fig. 3(b). Our data show that the degree of ordering tends to increase with aging, and the applied shear appears to further *amorphize/rejuvenate* the deforming glass (*eg.* by reduction in the icosahedral cluster density by $> 10\%$). Nevertheless, this observable, lacks a clear signature of the yielding transition and associated variations with age.

The D_{\min}^2 maps depicted in Fig. 2 give a visual impression that the elastic-plastic transition in BMGs (at $\gamma_{xy} \simeq 0.1$) might indeed coincide with a *percolation* transition of rearranging atoms upon shear loading (see also [29] and references therein). To validate this picture, we adopt ideas from classical percolation theory [38], including investigations of cluster sizes and their dynamical evolution. To perform the cluster analysis, atom-wise D_{\min}^2 was interpolated on a regular (cubic) grid and the top 5% of grid points with highest D_{\min}^2 were labeled as rearranging sites and colored in black in Fig. 4(a). As a basic statistical property, n_s denotes the probability distribution function associated with the number of clusters containing s rearranging sites. The radius of gyration associated with a cluster of size s is defined as $r_s^2 = \sum_{i=1}^s |\vec{r}_i - \vec{r}_0|^2 / s$ with the center of mass $\vec{r}_0 = \sum_{i=1}^s \vec{r}_i / s$. We obtain $s \propto r_s^{d_f}$ with fractal dimension d_f . The mean cluster size is defined as $S = \sum_s n_s s^2 / \sum_s n_s s$. We also define the (squared) correlation length $\xi^2 = 2 \sum_s r_s^2 s^2 n_s / \sum_s s^2 n_s$, based on a weighted average that is associated with the radius of gyration $r_s^2 = \sum_{i=1}^s |\vec{r}_i - \vec{r}_0|^2 / s$ of a cluster of size s .

The evolution of fractal dimension d_f with strain is illustrated in Fig. 4(b), corresponding to three different sample ages. The overall reduction towards $d_f = 2$ may imply that the soft spots tend to form fairly compact clusters at low strains but favor a more planar topology

on approach to yielding. Displayed in Fig. 4(c) and (d), both mean cluster size S and correlation length ξ indicate a fairly smooth evolution with strain at $t_{\text{age}} = 0$ but develop quite sharp features as the age is increased towards $t_{\text{age}} = 90$ ps. The correlation length tends to saturate at $\xi \simeq 45$ Å due to the physical size limit, in a visual agreement with cluster maps illustrated in Fig. 4(a) and (b). The overall reduction in size with increasing t_{age} at initial stages of deformation indicates that annealing and associated structural relaxation leads to annihilation of STZs, in contrast to the observed enhancement in the density of SROs (*cf.* Fig. 3(b)).

Conclusions – The present study of sheared BMGs has brought new insights into the underlying correlations between aging, structural ordering, and strain localization. We have presented direct evidence that the annealing process plays a pivotal role in controlling the sharpness of the shear-induced elastic-plastic transition, leading to a crossover from diffuse deformation features in as-quenched samples to localized shear-band-like patterns in well-annealed deforming glasses. Our findings suggest that the observed crossover is rooted in the interplay between aging-induced icosahedral ordering and collective formation of STZs. This observation has been quantified via probing several order parameters coupled with measurable dynamical and structural metrics. This includes fluctuations in the atoms' propensity to plastic rearrangements as well as spatial variations in the local density of icosahedral clusters. By analyzing connected networks of soft rearranging regions, we extracted relevant length scales that evolve across the yielding transition and exhibit significant variations with the sample's age. Our findings contribute to a better understanding of the complex interplay between structural order, aging, and plasticity in metallic glasses. This knowledge has implications for the design and optimization of metallic glasses for various engineering applications, whereas the control over strain localization and ductility via preparation protocols may be crucial.

Acknowledgments – This research was funded by the European Union Horizon 2020 research and innovation program under grant agreement no. 857470 and from the

-
- [1] A. Argon and H. Kuo, Plastic flow in a disordered bubble raft (an analog of a metallic glass), *Materials science and Engineering* **39**, 101 (1979).
- [2] M. L. Falk and J. S. Langer, Dynamics of viscoplastic deformation in amorphous solids, *Physical Review E* **57**, 7192 (1998).
- [3] M. L. Falk and J. S. Langer, Deformation and failure of amorphous, solidlike materials, *Annu. Rev. Condens. Matter Phys.* **2**, 353 (2011).
- [4] K. Karimi and J.-L. Barrat, Correlation and shear bands in a plastically deformed granular medium, *Scientific reports* **8**, 1 (2018).
- [5] M. Ozawa, L. Berthier, G. Biroli, A. Rosso, and G. Tarjus, Random critical point separates brittle and ductile yielding transitions in amorphous materials, *Proceedings of the National Academy of Sciences* **115**, 6656 (2018).
- [6] D. V. Denisov, K. A. Lórinicz, W. J. Wright, T. C. Hufnagel, A. Nawano, X. Gu, J. T. Uhl, K. A. Dahmen, and P. Schall, Universal slip dynamics in metallic glasses and granular matter—linking frictional weakening with inertial effects, *Scientific reports* **7**, 1 (2017).
- [7] K. Karimi, E. E. Ferrero, and J.-L. Barrat, Inertia and universality of avalanche statistics: The case of slowly deformed amorphous solids, *Physical Review E* **95**, 013003 (2017).
- [8] K. Karimi, D. Amitrano, and J. Weiss, From plastic flow to brittle fracture: Role of microscopic friction in amorphous solids, *Physical Review E* **100**, 012908 (2019).
- [9] Y. Cheng and E. Ma, Atomic-level structure and structure–property relationship in metallic glasses, *Progress in materials science* **56**, 379 (2011).
- [10] Y. Cheng, A. J. Cao, H. Sheng, and E. Ma, Local order influences initiation of plastic flow in metallic glass: Effects of alloy composition and sample cooling history, *Acta Materialia* **56**, 5263 (2008).
- [11] Y. Cheng, A. Cao, and E. Ma, Correlation between the elastic modulus and the intrinsic plastic behavior of metallic glasses: The roles of atomic configuration and alloy composition, *Acta Materialia* **57**, 3253 (2009).
- [12] H.-K. Kim, J.-P. Ahn, B.-J. Lee, K.-W. Park, and J.-C. Lee, Role of atomic-scale chemical heterogeneities in improving the plasticity of cu-zr-ag bulk amorphous alloys, *Acta Materialia* **157**, 209 (2018).
- [13] W. Li, P. Liu, and P. K. Liaw, Microstructures and properties of high-entropy alloy films and coatings: a review, *Materials Research Letters* **6**, 199 (2018).
- [14] Z. Li, S. Zhao, R. O. Ritchie, and M. A. Meyers, Mechanical properties of high-entropy alloys with emphasis on face-centered cubic alloys, *Progress in Materials Science* **102**, 296 (2019).
- [15] Y. Lu, Z. Zhang, X. Lu, Z. Qin, J. Shen, Y. Huang, and P. K. Liaw, Cooling-rate induced softening in a colloidal glass, *Scientific reports* **7**, 1 (2017).
- [16] N. Wang, J. Ding, F. Yan, M. Asta, R. O. Ritchie, and L. Li, Spatial correlation of elastic heterogeneity tunes the deformation behavior of metallic glasses, *npj Computational Materials* **4**, 1 (2018).
- [17] F.-F. Wu, Z.-F. Zhang, and S. X.-Y. Mao, Transition of failure mode and enhanced plastic deformation of metallic glass by multiaxial confinement, *Advanced Engineering Materials* **11**, 898 (2009).
- [18] M. Chen, A. Inoue, W. Zhang, and T. Sakurai, Extraordinary plasticity of ductile bulk metallic glasses, *Physical Review Letters* **96**, 245502 (2006).
- [19] K. Karimi, A. Esfandiarpour, R. Alvarez-Donado, M. J. Alava, and S. Papanikolaou, Shear banding instability in multicomponent metallic glasses: Interplay of composition and short-range order, *Physical Review B* **105**, 094117 (2022).
- [20] Y. Shi and M. L. Falk, Strain localization and percolation of stable structure in amorphous solids, *Physical review letters* **95**, 095502 (2005).
- [21] F. Albano and M. L. Falk, Shear softening and structure in a simulated three-dimensional binary glass, *The Journal of chemical physics* **122**, 154508 (2005).
- [22] J. Ding, Y.-Q. Cheng, and E. Ma, Full icosahedra dominate local order in cu64zr34 metallic glass and supercooled liquid, *Acta materialia* **69**, 343 (2014).
- [23] J. Ding, Y. Cheng, and E. Ma, Correlating local structure with inhomogeneous elastic deformation in a metallic glass, *Applied Physics Letters* **101**, 121917 (2012).
- [24] J. Ding, S. Patinet, M. L. Falk, Y. Cheng, and E. Ma, Soft spots and their structural signature in a metallic glass, *Proceedings of the National Academy of Sciences* **111**, 14052 (2014).
- [25] E. Ma and J. Ding, Tailoring structural inhomogeneities in metallic glasses to enable tensile ductility at room temperature, *Materials Today* **19**, 568 (2016).
- [26] Y. Shi and M. L. Falk, Atomic-scale simulations of strain localization in three-dimensional model amorphous solids, *Physical Review B* **73**, 214201 (2006).
- [27] Y. Shi and M. L. Falk, Stress-induced structural transformation and shear banding during simulated nanoindentation of a metallic glass, *Acta materialia* **55**, 4317 (2007).
- [28] T. C. Hufnagel, C. A. Schuh, and M. L. Falk, Deformation of metallic glasses: Recent developments in theory, simulations, and experiments, *Acta Materialia* **109**, 375 (2016).
- [29] K. Karimi, M. J. Alava, and S. Papanikolaou, Yielding in multicomponent metallic glasses: Universal signatures of elastic modulus heterogeneities, *Physical Review Materials* **7**, 063601 (2023).
- [30] See Supplemental Material at [URL will be inserted by publisher] for further discussions relevant to simulation details.
- [31] S. Plimpton, Fast parallel algorithms for short-range molecular dynamics, *Journal of computational physics* **117**, 1 (1995).
- [32] H. Ding and K. Yao, High entropy ti20zr20cu20ni20be20 bulk metallic glass, *Journal of non-crystalline solids* **364**, 9 (2013).
- [33] R. Alvarez-Donado, S. Papanikolaou, A. Esfandiarpour, and M. Alava, Viewing high entropy alloys through

- glasses: Linkages between solid solution and glass phases in multicomponent alloys, *Physical Review Materials* **7**, 025603 (2023).
- [34] W.-M. Choi, Y. H. Jo, S. S. Sohn, S. Lee, and B.-J. Lee, Understanding the physical metallurgy of the cocrfemni high-entropy alloy: an atomistic simulation study, *npj Computational Materials* **4**, 1 (2018).
- [35] A. Lees and S. Edwards, The computer study of transport processes under extreme conditions, *Journal of Physics C: Solid State Physics* **5**, 1921 (1972).
- [36] A. Stukowski, Visualization and analysis of atomistic simulation data with ovito—the open visualization tool, *Modelling and Simulation in Materials Science and Engineering* **18**, 015012 (2009).
- [37] K. Chen and K. S. Schweizer, Theory of yielding, strain softening, and steady plastic flow in polymer glasses under constant strain rate deformation, *Macromolecules* **44**, 3988 (2011).
- [38] D. Stauffer and A. Aharony, *Introduction to percolation theory* (Taylor & Francis, 2018).

Tuning brittleness in multi-component metallic glasses through chemical disorder aging

Kamran Karimi¹ and Stefanos Papanikolaou¹
¹ *NOMATEN Centre of Excellence,
National Center for Nuclear Research,
ul. A. Soltana 7, 05-400 Swierk/Otwock, Poland*

SUPPLEMENTARY MATERIALS

In this Supplementary Materials, we will provide additional details relevant to the preparation protocols of the CoNiCrFeMn, Co₅Cr₂Fe₄₀Mn₂₇Ni₂₆, CoNiCrFe, and CoNiFe metallic glasses presented in this study.

Simulations and Protocols

Molecular dynamics simulations were carried out in LAMMPS [1] by implementing atomistic systems of size $N = 50,688$ within periodic cubic boxes with $L \simeq 80$ Å in a simple-shear loading geometry. The above compositions are characterized by fairly low misfit coefficients δ_a and, therefore, low glass forming ability owing to effects of atomic size distributions. Nonetheless, there is a way to generate a model glass in the opposite limit of $\delta_a \rightarrow 0$ by maintaining a larger number of elements, as in medium/high entropy metallic glasses and/or using higher cooling rates (see [2, 3] and references therein).

The interatomic forces were derived from the modified embedded atom method (MEAM) potential with the input parameters associated with the principle elements obtained from [4]. The glassy samples were prepared based on the melt-and-quench protocol where a crystalline structure was initially heated up to a high temperature (3000 K) above the melting temperature $T > T_m$, before it was cooled down to the room temperature (300 K) below T_g at the quench rate of $\dot{T} = 0.1$ K/ps. We allowed for further relaxation upon quenching for order 10 ps to ensure as-quenched glasses are fully equilibrated prior to shearing. The ambient pressure P_0 was set to zero at all times. We also set the discretization time to $\Delta t = 0.001$ ps. The NPT ensembles were implemented via a Nose-Hoover thermostat and barostat with relaxation time scales $\tau_d^{\text{therm}} = 0.2$ ps and $\tau_d^{\text{bar}} = 2.5$ ps.

The annealing process was implemented through Monte Carlo swaps between atoms of different types at a specified (annealing) temperature $T_a = 300$ K, the (attempted) swapping rate of 10^4 pairs per ps, and over the aging duration of $t_{\text{age}} = 100$ ps. Figure S1 plots the accepted swapping rate, volume, and mean number density of atoms with icosahedral symmetry $\langle \rho_{\text{ico}} \rangle$ as a function of annealing time t_{age} in Co₅Cr₂Fe₄₀Mn₂₇Ni₂₆. A strain-controlled condition was applied by deforming the

periodic box on the xy plane implementing Lees-Edwards boundary conditions [5] at a fixed volume and temperature (canonical NVT ensembles) and a constant shearing rate $\dot{\gamma}_{xy} = 10^{-4}$ ps⁻¹ up to a 20% strain. Figure S2 displays macroscopic stress σ_{xy} against applied (shear) strain γ_{xy} at several aging duration t_{age} corresponding to Co₅Cr₂Fe₄₀Mn₂₇Ni₂₆, CoNiCrFe, and CoNiFe. We further measure the softening modulus h_{min} defined as the maximum rate of the macroscopic stress drop at every age t_{age} as in Fig. S3.

Results

Dynamics of individual atoms is quantified by D_{min}^2 as a measure of deviations from affine trajectories of atoms imposed by an external (homogeneous) shear [6]. The D_{min}^2 analysis involves partitioning of the entire box into sub-volumes using a cubic grid of size $r_c = 3.0$ Å. We fit a linear model based on the reference positions \vec{r} at zero strain, i.e. $\vec{\mathcal{R}}(\vec{r}) = \mathbf{F}\vec{r} + \vec{F}_0$, to the current atomic positions \vec{r} associated with N_b atoms within a given volume by minimizing the squared loss function $\mathcal{L}(\mathbf{F}, \vec{F}_0) = \sum_{i=1}^{N_b} |\vec{r}_i - \vec{\mathcal{R}}(\vec{r}_i)|^2$ to obtain $\{\hat{\mathbf{F}}, \hat{\vec{F}}_0\} = \text{argmin} \mathcal{L}(\mathbf{F}, \vec{F}_0)$. Here the second-ranked deformation tensor \mathbf{F} and the (rigid) translation vector \vec{F}_0 correspond to an affine transformation. The squared nonaffine displacements for atom i is defined as $D_i^2 = |\vec{r}_i - \hat{\vec{r}}_i|^2$ with $\hat{\vec{r}}_i$ being the predicted position $\hat{\vec{\mathcal{R}}}(\vec{r}) = \hat{\mathbf{F}}\vec{r} + \hat{\vec{F}}_0$ due to affine deformations.

Figure S4 plots the evolution of correlation coefficient c_{XY} , mean number density of atoms with icosahedral symmetries $\langle \rho^{\text{ico}} \rangle$, mean squared nonaffine displacements $\langle D_{\text{min}}^2 \rangle$, and scaled standard deviation $\text{std}(D_{\text{min}}^2) / \langle D_{\text{min}}^2 \rangle$ associated with atoms' D_{min}^2 against applied strain γ_{xy} in Co₅Cr₂Fe₄₀Mn₂₇Ni₂₆ corresponding to different aging duration t_{age} . Figure S5 displays fractal dimension d_f , mean cluster size S , and correlation length ξ plotted against strain γ_{xy} at multiple age t_{age} corresponding to Co₅Cr₂Fe₄₀Mn₂₇Ni₂₆.

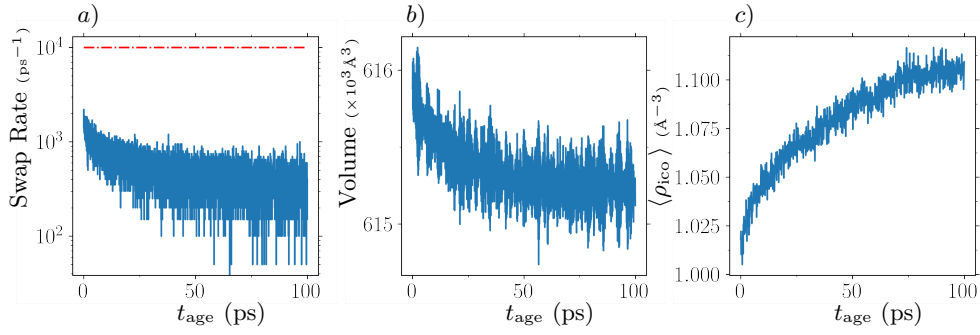


FIG. S1. **a)** Accepted swapping rate **b)** volume **c)** mean number density of atoms with icosahedral symmetry $\langle \rho_{\text{ico}} \rangle$ plotted against aging duration t_{age} in $\text{Co}_5\text{Cr}_2\text{Fe}_{40}\text{Mn}_{27}\text{Ni}_{26}$. The red flat line indicates the attempted swapping rate.

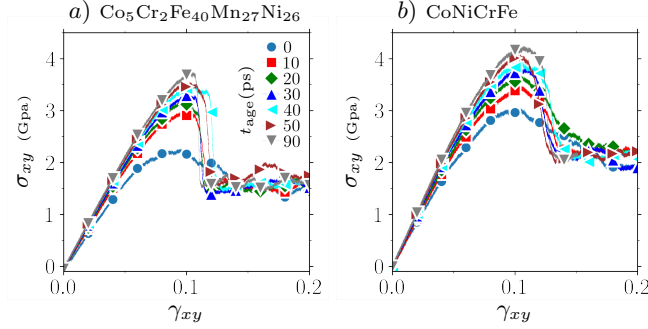


FIG. S2. Macroscopic stress σ_{xy} plotted against applied (shear) strain γ_{xy} at several aging duration t_{age} corresponding to **a)** $\text{Co}_5\text{Cr}_2\text{Fe}_{40}\text{Mn}_{27}\text{Ni}_{26}$ **b)** CoNiCrFe .

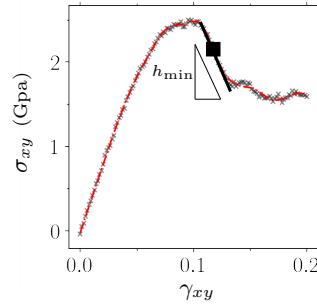


FIG. S3. Illustration of the softening modulus h_{min} . The (black) crosses indicate the stress data points σ_{xy} as a function of the applied (shear) strain γ_{xy} . The dashdotted (red) curve denotes a nonlinear fit based on (cubic) smoothing splines. The square symbol indicates the strain corresponding to the minimal slope past the stress peak as illustrated by the straight line.

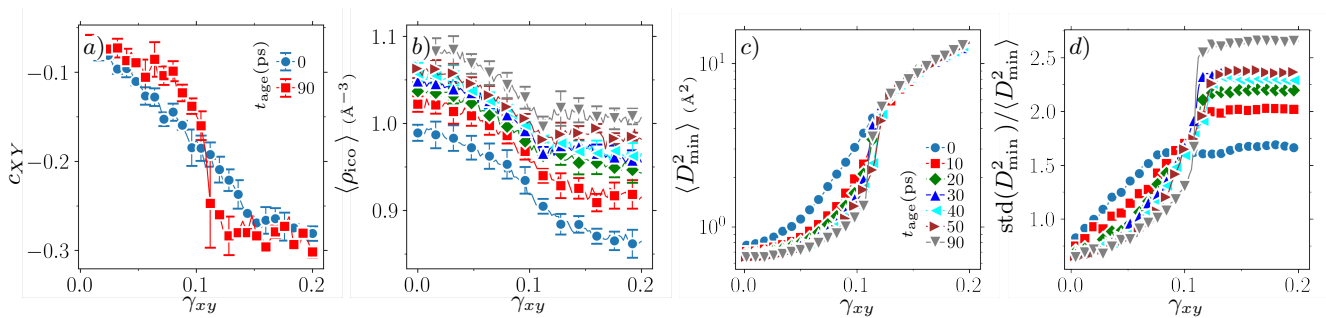


FIG. S4. Evolution of **a)** correlation coefficient c_{XY} **b)** mean number density of atoms with icosahedral symmetries $\langle \rho_{\text{ico}} \rangle$ **c)** mean squared nonaffine displacements $\langle D_{\text{min}}^2 \rangle$ **d)** scaled standard deviation $\text{std}(D_{\text{min}}^2) / \langle D_{\text{min}}^2 \rangle$ associated with atoms' D_{min}^2 plotted against applied strain γ_{xy} in $\text{Co}_5\text{Cr}_2\text{Fe}_{40}\text{Mn}_{27}\text{Ni}_{26}$ corresponding to different aging duration t_{age} . The error bars denote standard errors.

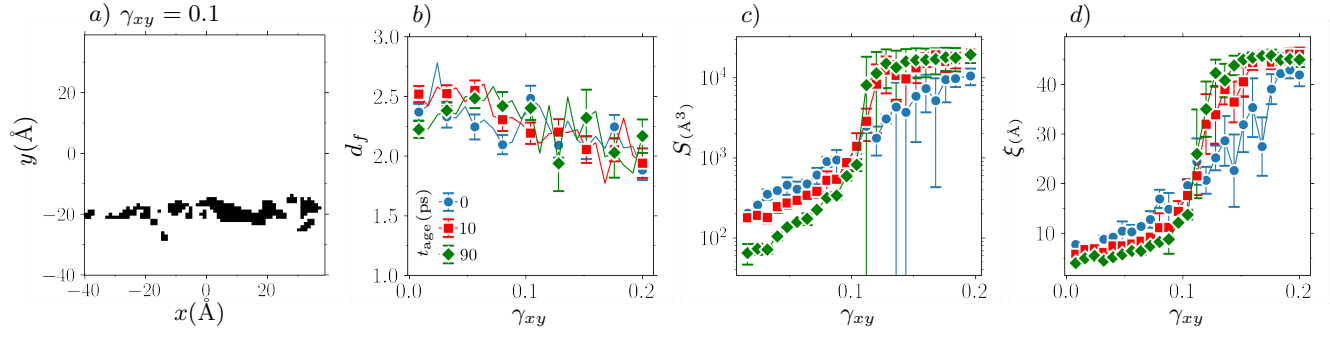


FIG. S5. **a)** Binary D_{\min}^2 map at $\gamma_{xy} = 0.1$ corresponding to the annealed $\text{Co}_5\text{Cr}_2\text{Fe}_{40}\text{Mn}_{27}\text{Ni}_{26}$ at $t_{\text{age}} = 90$ ps. **b)** Fractal dimension d_f **c)** Mean cluster size S **d)** Correlation length ξ plotted against strain γ_{xy} at multiple age t_{age} . Here x and y denote flow and gradient directions, respectively. The binary maps show top 5% sites with largest D_{\min}^2 in black.

-
- [1] S. Plimpton, Fast parallel algorithms for short-range molecular dynamics, *Journal of computational physics* **117**, 1 (1995).
- [2] H. Ding and K. Yao, High entropy ti20zr20cu20ni20be20 bulk metallic glass, *Journal of non-crystalline solids* **364**, 9 (2013).
- [3] R. Alvarez-Donado, S. Papanikolaou, A. Esfandiarpour, and M. Alava, Viewing high entropy alloys through glasses: Linkages between solid solution and glass phases in multicomponent alloys, *Physical Review Materials* **7**, 025603 (2023).
- [4] W.-M. Choi, Y. H. Jo, S. S. Sohn, S. Lee, and B.-J. Lee, Understanding the physical metallurgy of the cocr-femni high-entropy alloy: an atomistic simulation study, *npj Computational Materials* **4**, 1 (2018).
- [5] A. Lees and S. Edwards, The computer study of transport processes under extreme conditions, *Journal of Physics C: Solid State Physics* **5**, 1921 (1972).
- [6] M. L. Falk and J. S. Langer, Dynamics of viscoplastic deformation in amorphous solids, *Physical Review E* **57**, 7192 (1998).